Sensors and Actuators Reports 4 (2022) 100083

Contents lists available at ScienceDirect

Sensors and Actuators Reports

journal homepage: www.sciencedirect.com/journal/sensors-and-actuators-reports

Detection of *Staphylococcus aureus* in milk samples using impedance spectroscopy and data processing with information visualization techniques and multidimensional calibration space.

Juliana Coatrini Soares [1,2], Andrey Coatrini Soares [1], Mario Popolin-Neto [3,4], Fernando Vieira Paulovich [3,5], Osvaldo N. Oliveira Jr [2,*], Luiz Henrique Caparelli Mattoso [1]

[1] *Embrapa Instrumentação, Nanotechnology National Laboratory for Agriculture (LNNA), São Carlos, Brazil*
[2] *São Carlos Institute of Physics (IFSC), University of São Paulo (USP), 13566-590 São Carlos, Brazil*
[3] *Institute of Mathematics and Computer Sciences (ICMC), University of São Paulo (USP), 13566-590 São Carlos, Brazil*
[4] *Federal Institute of São Paulo (IFSP), 14804-296 Araraquara, Brazil*
[5] *Faculty of Computer Science (FCS), Dalhousie University (DAL), B3H 4R2 Nova Scotia, Canada*

ARTICLE INFO

Keywords:
Staphylococcus aureus
Mastitis
immunosensor
nanostructured film
machine learning

ABSTRACT

Early diagnosis of cattle diseases such as mastitis caused by *Staphylococcus aureus* (*S. aureus*) can be made effective if on-site detection methods with portable instruments are available. In this work, we fabricated immunosensors based on a layer-by-layer (LbL) film of chitosan and carbon nanotubes coated with a layer of antibodies to detect *S. aureus*. Using electrical and electrochemical impedance spectroscopies, detection was possible in buffer solutions and in milk with limits of detection which could be as low as 2.6 CFU/mL for milk, sufficient to detect mastitis at early stages. This high sensitivity is ascribed to the specific interactions involving the antibodies, as demonstrated with polarization-modulated infrared reflection absorption spectroscopy (PM-IRRAS). The selectivity of the immunosensor was verified by distinguishing *S. aureus*-containing samples from possible interferents found in milk, for which the interactive document mapping (IDMAP) was employed. Because the interferents affected the spectra, in spite of this distinguishability, we treated the data with a machine learning technique with decision tree models. A multidimensional calibration space was then obtained with rules that permit interpretability and predictability in detecting *S. aureus* in matrices with high variability as in milk.

1. Introduction

Detection of *Staphylococcus aureus* (*S. aureus*) in milk is relevant for diagnosing mastitis, one of the most frequent and costly diseases in dairy cows as it leads to severe milk loss, decreased milk quality, and increased probability of cow death [1]. While clinical mastitis may be readily recognized with a visual inspection of the mammary gland and milk, the same does not apply to subclinical mastitis which hinders an early diagnosis [2]. Such diagnosis can be done indirectly if the presence of *S. aureus* is detected in the milk at early stages of the disease. The most used method to diagnose intramammary infections is polymerase chain reaction (PCR) [3,4], which is accurate for bacterial DNA detection from bovine milk. However, this test is expensive due to the experimental procedures and equipment required [5]. Other tests include somatic cell count (SCC) [6], lactose percentage in mastitis milk [7], lactate dehydrogenase (LDH) test in mammalian tissues [8], electricity conductivity (EC) of milk [9] and N-acetyl-β-D-glucosaminidase test (NAGase) in milk from damaged breast epithelial cells [10]. Considering cost and ease of data collection, immunosensor devices are the most appropriate diagnostic test for detecting subclinical mastitis [11]. Immunosensors can be based on different detection principles, including impedance spectroscopy [12,13], colorimetry [14] and photoelectrochemical methods [15]. With the latter, photoactive materials and signal strategies may be chosen to reach high sensitivity and selectivity. Such photoelectrochemical methods have been used in monitoring food quality, as in the detection of mycotoxins [15,16]. It is relevant that colorimetric immunoassays were suitable to detect neurotoxins with high sensitivity, which was made possible by combining glucose oxidase and gold

* Corresponding Author.
E-mail address: chu@ifsc.usp.br (O.N. Oliveira).

https://doi.org/10.1016/j.snr.2022.100083
Received 17 November 2021; Received in revised form 13 January 2022; Accepted 30 January 2022
Available online 4 February 2022

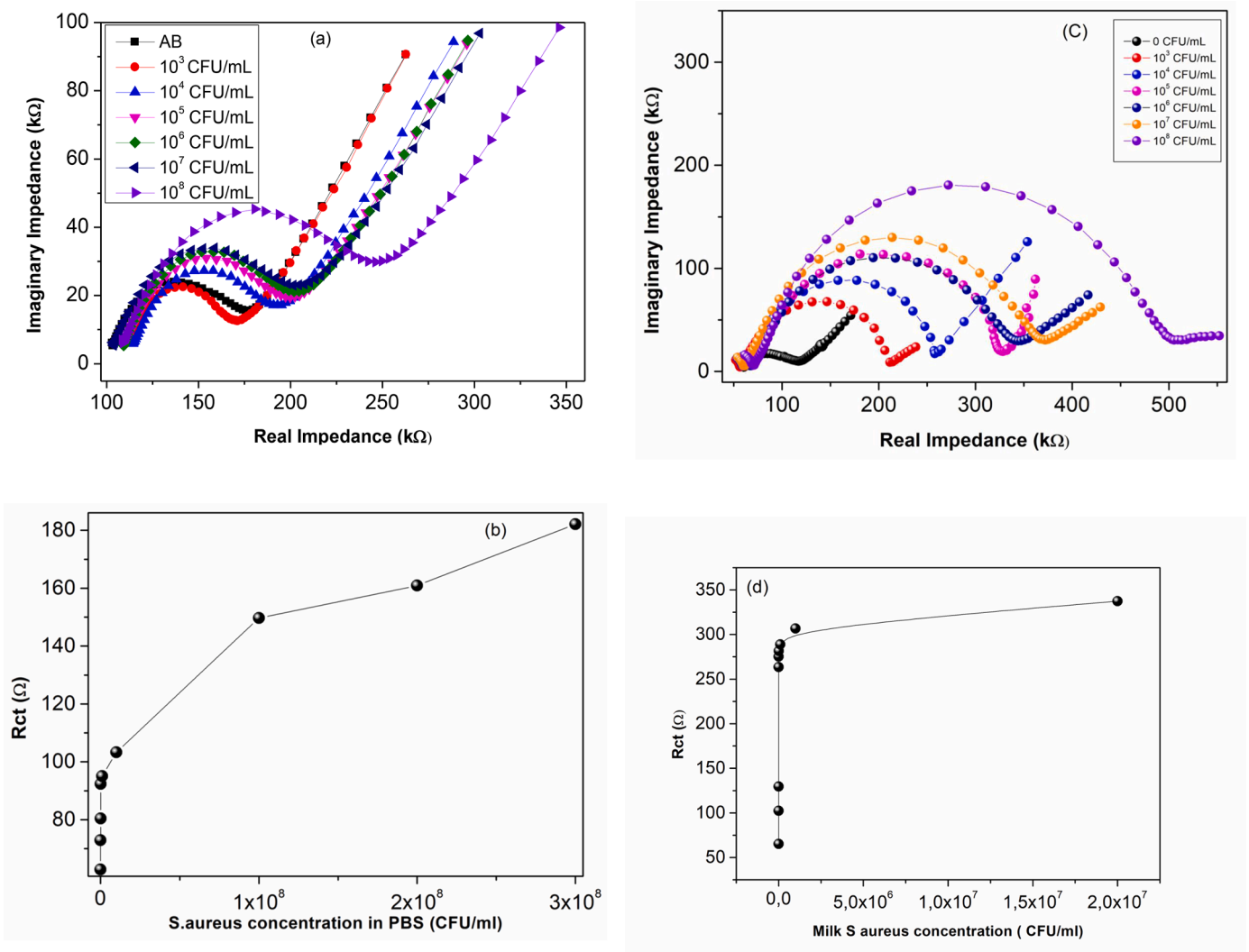

Fig. 1. (a) and (c) Nyquist plots of the impedance spectra from 100 kHz to 1 Hz for a gold electrode modified with a CHT/MWCNT/anti-*S.aureus*-BSA exposed to varying concentrations of the S aureus samples and milk sample in $K_3Fe(CN)_6$ and $K_4Fe(CN)_6$ (5mmol/L). (b) and (d) Plots of the relative change in R_{ct} against the concentration of S *aureus* samples and milk solution in $K_3Fe(CN)_6$ and $K_4Fe(CN)_6$ (5 mmol/L).

nanoparticles functionalized with antibodies in the signal transduction tag [14].

Immunosensors are now mostly fabricated with nanostructured films that incorporate a biomolecule to interact specifically with the analyte of interest. These films may be produced with self-assembled monolayers (SAMs) [17,18], layer by-layer (LbL) films [19,20], which are suitable for preserving the activity of the immobilized biomolecules [21]. They can contain nanomaterials such as carbon nanotubes, graphene, carbon dots and nanosheets [22]. There are several possible functions for the nanomaterials used in immunosensors. Perhaps the most relevant are related to enhancing the sensing signal via synergy with the biomolecules [23] and increasing the surface area of the working electrode in electrochemical devices [24]. Carbon nanotubes, in particular, have been proven excellent to increase surface roughness and then the sensitivity[25].

In this work we exploit the advantages of immunosensors based on electrical and electrochemical impedance spectroscopy to detect S. *aureus* in milk and commercial samples. The immunosensor is a nanostructured film that contains a matrix of chitosan and carbon nanotubes, coated with a layer of Anti-*S. aureus* antibodies to recognize S. *aureus* specific sites. High sensitivity and selectivity are obtained, especially by employing information visualization. Furthermore, using machine learning methods it was possible to establish rules that afford some degree of predictability in the biosensing task.

2. Methodology

2.1. Immunosensor Fabrication

The immunosensors were made with layer-by-layer (LbL) [26,27] films of chitosan (CHT) and carbon nanotubes (Sigma Aldrich) modified with carboxylic acids (MWCNT) [28,29] (Sigma-Aldrich). LbL films were obtained by depositing a chitosan layer from a 1 g/mL solution in acetate buffer pH 4.5 either onto a gold electrode (Zimmer & Peacock A/S, Coventry, England) or interdigitated gold electrode during 10 min, followed by immersion into the MWCNT solution for 20 min. The former gold electrode was used for electrochemical measurements in phosphate buffer saline (PBS) (Sigma-Aldrich) solutions while for the electrical impedance measurements the interdigitated gold electrodes had 50 pairs of 10 μm wide digits with 10 μm spacing between them. The active layer was deposited onto the LbL films by first immobilizing N-ethyl-N-(3-dimethylaminopropyl) carbodiimide (EDC) and N-hydroxysuccinimide (NHS), acquired from Sigma-Aldrich, with a 0.1 mol/L EDC:NHS (1:1) solution to modify the MWCNT carboxylic acids. Then, anti–*S. aureus* antibodies in which the host species is a rabbit (ABCAM-ab20920)) were adsorbed as the top layer. In order to avoid

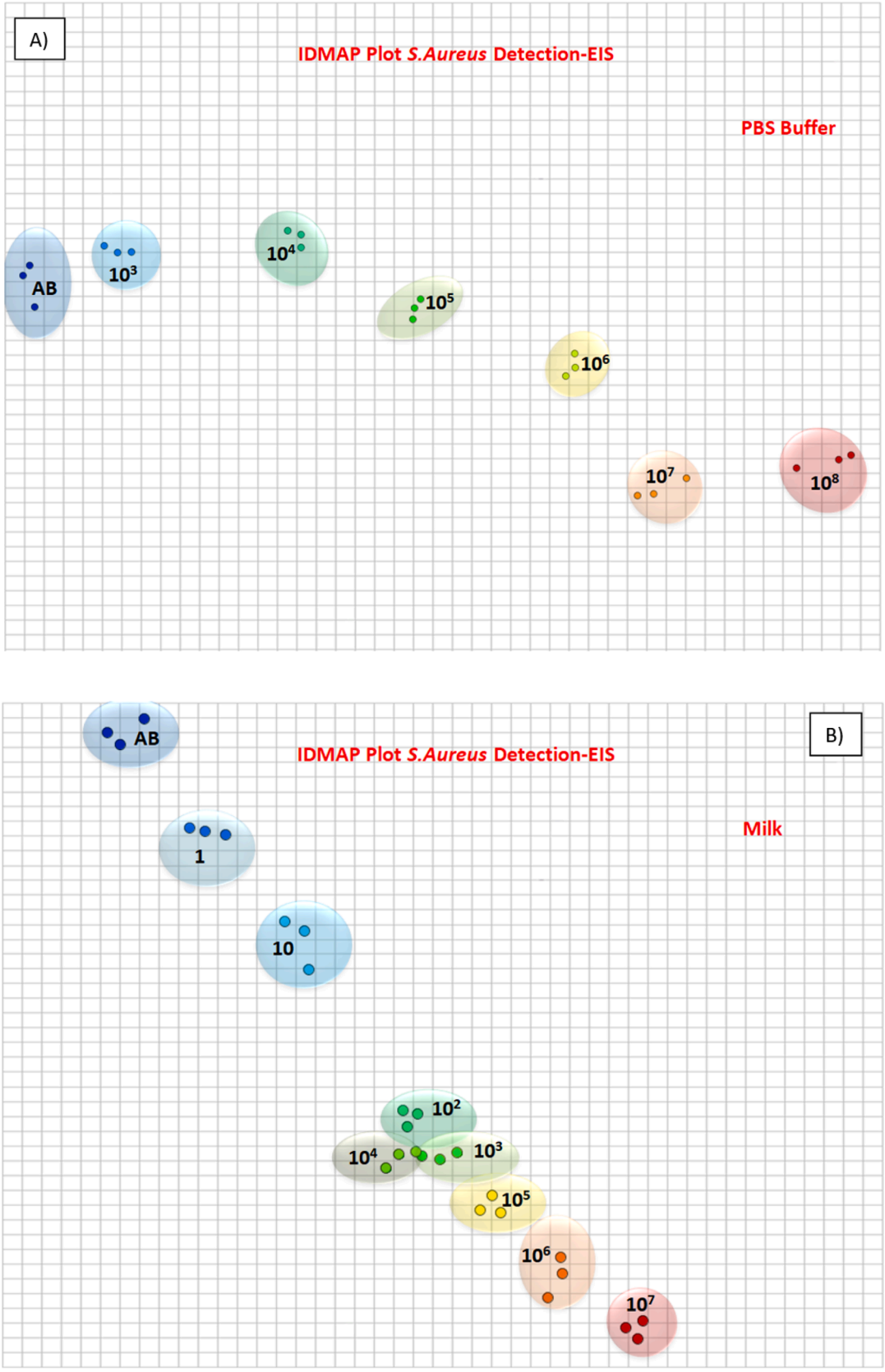

Fig. 2. IDMAP plots obtained with the EIS spectra for the immunosensor exposed to different concentrations of *S. aureus* in (a) PBS solutions; (b) milk. The maps have no axes because what is relevant in these plots is the relative distance between data points.

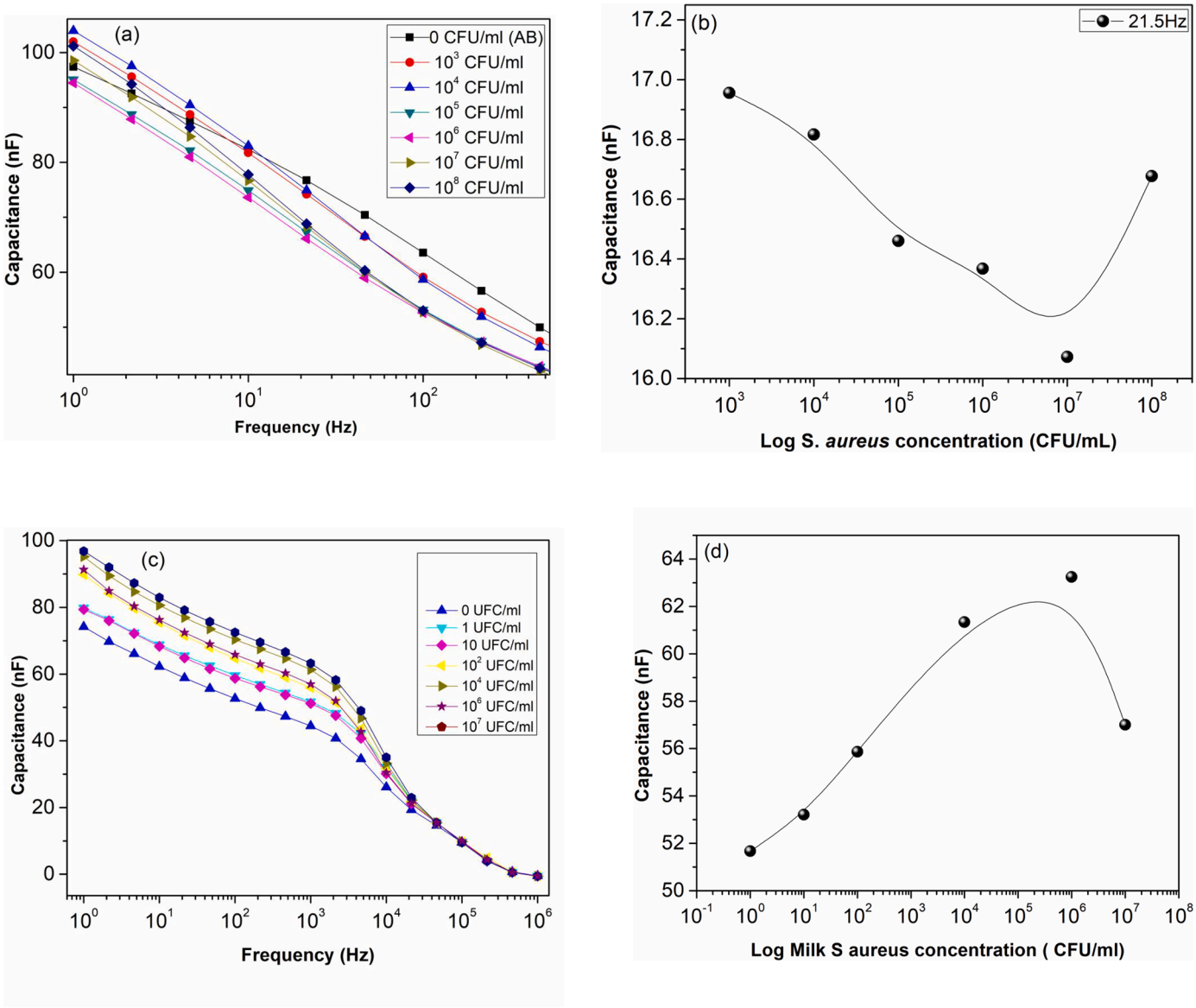

Fig. 3. Capacitance spectra for CHT/MWCNT/anti-*S.aureus*-BSA exposed to various concentrations of S.*aureus* in (a) PBS solutions and (c) milk and calibration curves for CHT/MWCNT/anti-*S. aureus*-BSA sensors exposed to various concentrations of S. *aureus* in (b) PBS solutions and (d) milk

non-specific adsorption in the detection experiments, the immunosensor were completed with incorporation of bovine serum albumin (BSA) 1% from Sigma-Aldrich by dropping a solution on the electrode for 15 min, which was then washed and dried. The film-forming process was monitored with polarization-modulated infrared reflection absorption spectroscopy (PM-IRRAS) in a KSV spectrophotometer, model PMI 550 (KSV Instruments, Finland), with spectral resolution of 8 cm^{-1} and at an incident angle of 81° [29–31]. From the electrochemical impedance spectroscopy (EIS) measurements, the resistance change was determined for each adsorbed layer of chitosan (CHT), carbon nanotubes (MWCNT), and antibodies (Anti-*S. aureus*), in addition to that caused by detection of *S. aureus*.

2.2. Detection of S. aureus

Samples of *S. aureus* were diluted in PBS solutions at concentrations ranging from 10^3 to 10^8 CFU/mL. For each bacteria concentration, an immunosensor unit was immersed in 50 μL of solution for 10 min. Following adsorption, the immunosensor was washed to eliminate or minimize non-specific adsorption. The same procedure was used for detection in milk samples (Letti A^2, Brazil), including fat content). Two methods were used for detection: impedance spectroscopy using a Solartron model 1260 A (Solartron Analytical, USA), in the range between 10^2 and 10^6 Hz, and electrochemical impedance spectroscopy (EIS) with an AnaPOT potenciostat from Zimmer & Peacock A/S. The latter measurements were made in a three-electrode configuration: the nanostructured film was deposited onto the gold interdigitated electrode as the working electrode (geometric area 9.5 mm^2), the reference electrode was Ag/AgCl (3 mol/L KCl) and the auxiliary electrode was made of gold (1.0 cm^2). EIS data were acquired in the frequency range between 0.1 Hz and 100 kHz with an amplitude of 10 mV and under open circuit conditions in a solution containing 5.0 mmol/L of $K_3[Fe(CN)_6]$/$K_4[Fe(CN)_6]$ (Sigma-Aldrich, USA).

2.3. Data Analysis with Visualization Techniques and Multidimensional Calibration Spaces

The capacitance spectra were analyzed with the multidimensional projection referred to as interactive document mapping (IDMAP) [32] to study selectivity and possible false positives in detecting *S. aureus*.

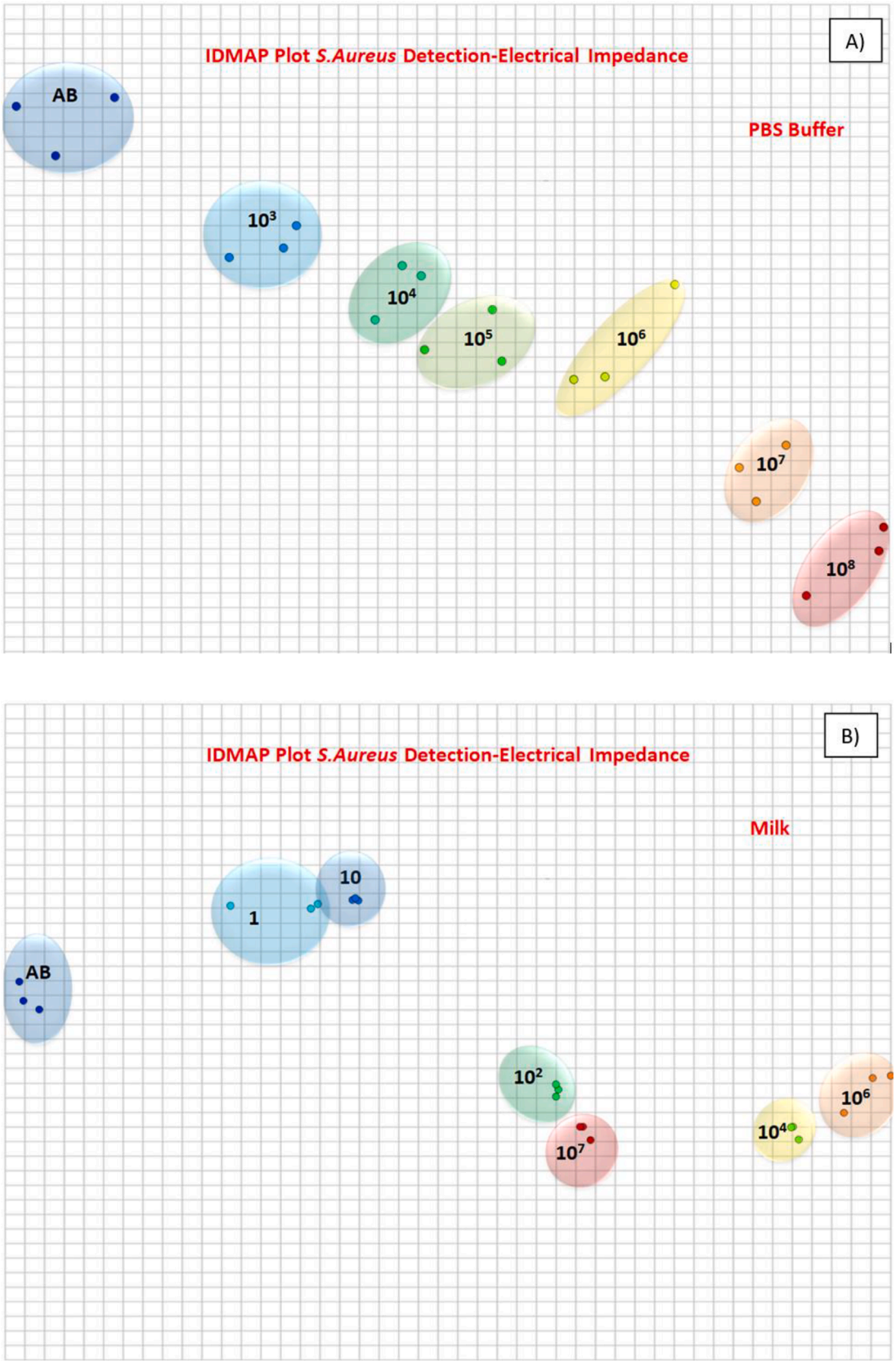

Fig. 4. IDMAP plots obtained with the electrical impedance spectra of Fig. 4 for the immunosensor exposed to different *S. aureus* concentrations in (a) PBS solutions, (b) milk.

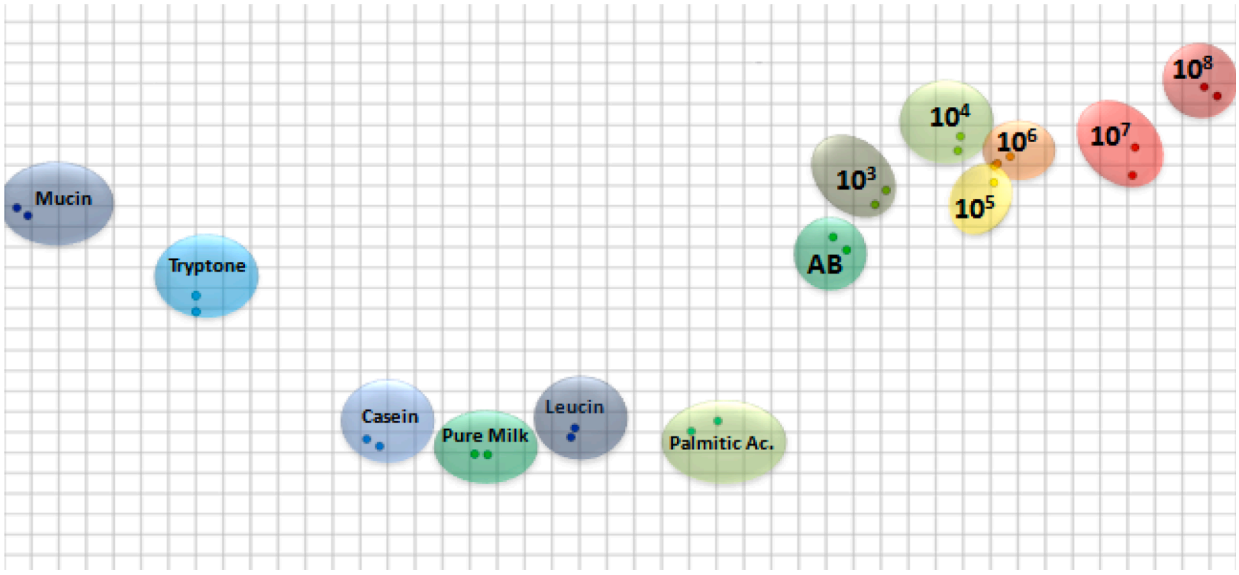

Fig. 5. IDMAP plot for the Electrical Impedance Spectra from interferents and milk solution in PBS and S. *aureus* antibody (AB).

IDMAP considers the Euclidean distance between the electrical signal of different S. aureus concentrations in the original space X={x_1, x_2, …,x_n} and projects them in a space of a lower dimension, where Y={y_1, y_2,…, y_n) gives the position of visual elements representing the spectra. Since information is inevitably lost in procedures to reduce data dimensions, the process was optimized using eq. 1,

$$S_{IDMAP} = \frac{\delta(x_i, x_j) - \delta_{\min}}{\delta_{\max} - \delta_{\min}} - d(y_i, y_j) \quad (1)$$

where $\delta(x_i,x_j)$ are the Euclidean distances in the original space, $d(y_i,y_j)$ are the Euclidean distances in the lower dimension space (2D in our case), and δ_{max} and δ_{min} are maximum and minimum Euclidean distances between the data instances.

A multidimensional calibration space (MCS) [33] was created from the capacitance values and concentrations taken as classes [34] using the interpretability represented with ExMatrix [35] applied for Decision Tree (DT) models [36–38]. Since these models are parametrized, a selection experiment [38] was performed through a KFold Cross-Validation [39], from which hyperparameter combinations were selected to maximize performance (i.e. accuracy). The models built with distinct hyperparameters were evaluated during the KFold Cross-Validation, and the hyperparameters providing the highest average performance were employed to create the final model. The Nested KFold Cross-Validation approach [40,41] was adopted for the performance estimation where an inner KFold Cross-Validation loop was executed for selecting the models (i.e. tuning the hyperparameters) [38]. The model performance was then carried out by an outer KFold Cross-Validation loop [40,41]. Optimistic (overestimation) and biased performance can be an issue on small datasets [40,41], as is the case of the dataset employed in this paper. These problems were avoided by using this Nested KFold Cross-Validation combined with the tuning of hyperparameters.

3. Results and Discussion

The building of the immunosensors film architecture was monitored with EIS and PM-IRRAS. The Nyquist diagrams in Fig. S1 in the Supporting Information show a considerable change in impedance when the layer of anti-*S. aureus* antibodies was adsorbed. Also shown are the changes in the diagrams when the immunosensors are exposed to two concentrations of bacteria. The adsorption of anti-*S. aureus* was confirmed with typical bands in the PM-IRRAS spectra of Fig. S2, [42–48] which also allowed us to infer the molecular-level interactions responsible for detection when the immunosensor was exposed to *S. aureus* in a PBS solution and in milk. The PM-IRRAS spectra feature bands at 1070, 1550 and 1655 cm^{-1} due to phospholipids, membrane proteins, other proteins, and antibodies. The bands assigned to C-H dipoles from CH_3 and CH_2 [49] in other milk components (such as lactose) are observed at 2859 cm^{-1} and 2935 cm^{-1}. The assignment of the main bands is given in Table S1 in the Supporting Information.

The detection of *S. aureus* was performed in triplicate, with two analytical methods, *viz.* electrical impedance spectroscopy and electrochemical impedance spectroscopy. The Nyquist plots in Fig. 1 depict the *S. aureus* detection in PBS solutions and in milk solution, whose data were analyzed using a Randles circuit comprising an electrolyte resistance (Rs), a charge transfer resistance (Rct) and a constant phase element (CPE). The change in Rct (in modulus) increases with the concentration of *S. aureus* in PBS and in milk, as indicated in Figs. 1b and 1d, respectively. At high concentrations the signal tends to saturate as all the sites available for interaction are taken. The detection limits were calculated from the initial linear range and using the IUPAC method (LOD = 3 SD/S), where SD is the standard deviation of 10 measurements taken from the blank signal and S is the slope of the analytical curve. These limits are 10 CFU/mL for PBS and 1.8 CFU/mL for milk, with the response tending to saturate at ca. 10^8 CFU/mL. This LOD is sufficient to detect mastitis at early stages, because the cutoff limit for latent mastitis is 1×10^4-1.2×10^4 CFU/mL [50]. The lower LOD for milk may indicate that this matrix (composed with proteins and fat) does not affect the activity of membrane proteins of bacteria which are recognized by the antibodies in the immunosensor. On the contrary, milk seems an even easier matrix than PBS to detect *S. aureus*, and this conclusion is corroborated with the results for impedance spectroscopy to be presented later on.

The distinction ability for the different concentrations of *S. aureus* in PBS solutions and in milk using EIS is better illustrated in the IDMAP plots in Figs. 2a and 2b, respectively. In these maps, each EIS spectrum is represented as a marker on the projected 2D chart. Samples with similar spectra are located close to each other, while very dissimilar samples are placed far apart. Note that the data points are shifted to the right with increasing concentrations. However, samples with 10^4 CFU/mL (Fig. 2b) are not correctly located, because the distinguishing ability using IDMAP is not perfect. Thus, we resorted to machine learning in section 3.1, which allowed for a higher accuracy in prediction

The effects from *S. aureus* on the capacitance values of the

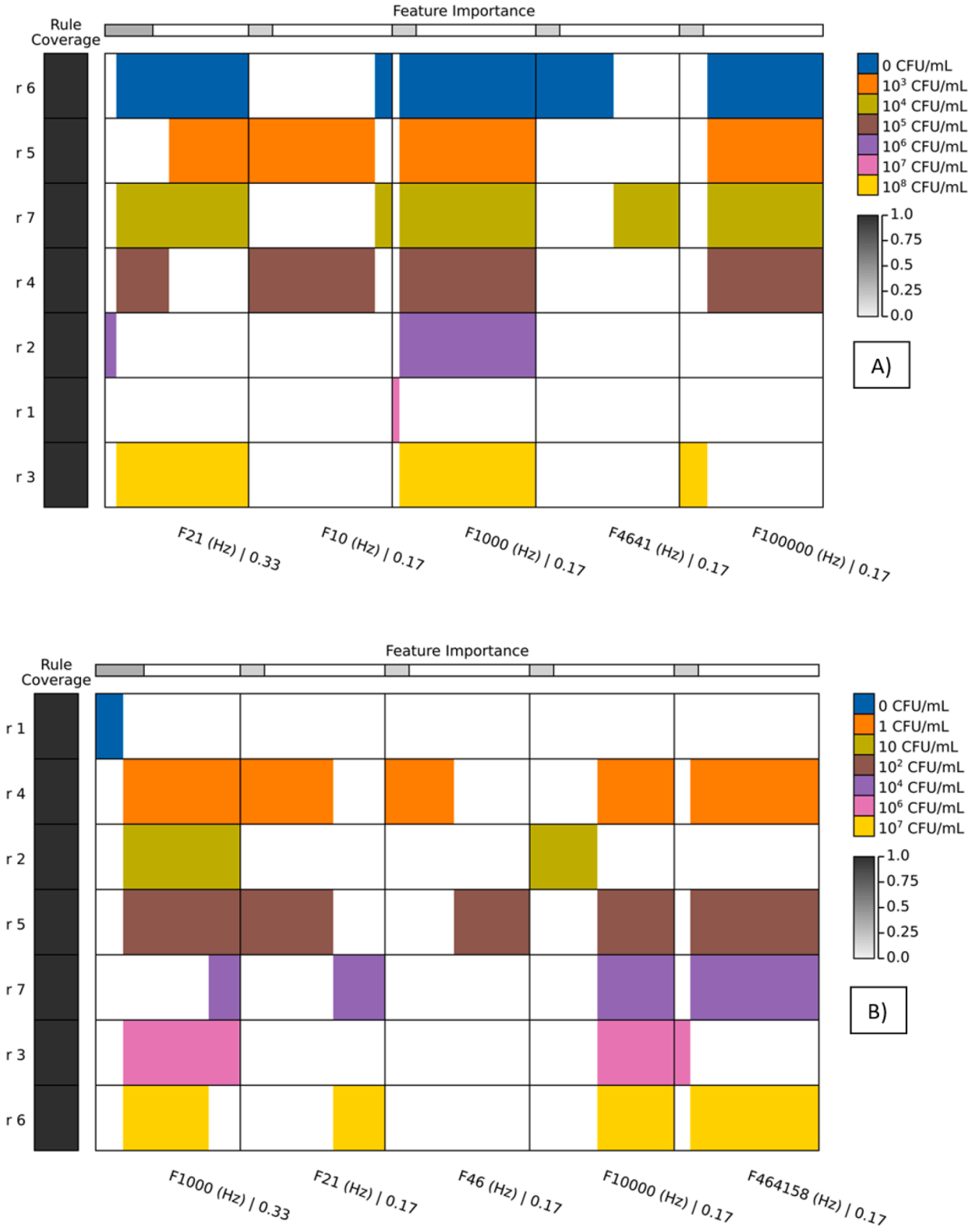

Fig. 6. Multidimensional Calibration Space (MCS) from two DT models in the ExMatrix representation, for PBS solutions (a) and milk samples (b). The logic rules presented in both spaces have the minimum number of rules (7, one per concentration class). For PBS solutions, the concentrations 0, 10^3, 10^4, 10^5, 10^6, 10^7, and 10^8 CFU/mL were discretized as classes. MCS has 5 dimensions corresponding to the 5 selected frequencies (features), which are 21 Hz, 10 Hz, 1000 Hz, 4641 Hz and 100000 Hz. The most important feature is F21, with an importance value of 0.33. The rules employ frequencies from different regions to distinguish the *S.aureus* concentrations, with the exception of rule r1 (sixth row) for 10^7 CFU/mL (magenta) which requires only F1000 Hz (third column). For the milk samples, the concentrations 0, 1, 10, 10^2, 10^4, 10^6, and 10^7 CFU/mL were discretized as classes, and MCS also has 5 dimensions, corresponding to F1000, F21, F46, F10000 and F464158. The most important feature is F1000, with an importance value of 0.33. As in the PBS solutions, different frequency regions are used in the rules except for 0 CFU/mL (blue) determined with rule r1 (first row) using F1000 Hz (first column).

immunosensors as measured with electrical impedance spectroscopy depend on the matrix. Fig. 3a shows that in PBS solutions the capacitance shows an overall decrease with increasing concentrations of *S. aureus* (according to the analytical curve in Fig. 3b). In contrast, the capacitance increases when the bacteria are in milk samples, as shown in Figs. 3c and 3d, where saturation is observed at high concentrations. The limit of detection estimated from the initial linear range using the IUPAC method (LOD = 3SD/S)[51] was 2.75 CFU/mL for commercial and 2.6 CFU/mL for milk. As in the case of EIS, a lower LOD was observed in milk samples.

Fig. 4 shows the IDMAP plots obtained from the impedance spectra in Fig. 3, where the distinction of the various *S. aureus* concentrations is demonstrated both for PBS solutions and milk. Because the impedance is very sensitive to any changes in the immunosensor, including from non-specific interactions, it is essential to verify whether false positives may occur. We have therefore made several control experiments in which the immunosensor was exposed to interferents, namely mucin, tryptone, casein, leucine, and palmitic acid, some of which can be found naturally in milk. The IDMAP plot in Fig. 5 confirms the selectivity of the immunosensor toward *S. aureus* in PBS solutions, whose data points occupy a distinct region of the plot compared to those of the interferents. This is despite the effects caused by such interferents – probably owing to non-specific adsorption – as it is clear in the IDMAP plot. Therefore, using this multidimensional projection technique one may obtain a reasonable distinction ability for the immunosensor, even in the presence of non-specific adsorption.

3.1. Machine Learning Applied to the Electrical Impedance Spectroscopy Data

The robustness of a monitoring system for detecting bacteria in real samples, as with milk investigated here, depends not only on a high sensitivity that can prevent false negatives but also on whether false positives can be avoided by distinguishing possible signals from interferents in the sample. We have shown that using the multidimensional projections techniques such as IDMAP may solve this problem. Still, this approach does not permit predictability when a new set of measurements are taken with real samples (e.g. milk) that exhibit an intrinsic variability. Such predictability may be afforded if the data are treated with supervised machine learning methods based on decision trees [36–38]. This was done here by creating two multidimensional calibration spaces (MCS) [33], one from capacitance spectra of PBS solutions and another from capacitance spectra of milk samples. The concentrations were discretized [34] as classes, resulting in 7 classes: 0, 10^3, 10^4, 10^5, 10^6, 10^7, and 10^8 CFU/mL for PBS solutions, and 0, 1, 10, 10^2, 10^4, 10^6, and 10^7 CFU/mL for milk samples. Both MCS were obtained using a model selection experiment [38] with a KFold Cross-Validation [41]. Several Decision Tree (DT) [36–38] models were built to select the DT hyperparameter combination yielding the highest average performance (i.e. accuracy) in a KFold Cross-Validation with k = 3. The chosen hyperparameters were used to create the final DT model and the MCS via ExMatrix visualization method [35]. To assess the performance of the DT model, a 3×2 Nested KFold Cross-Validation (k_outer = 3 and k_inner = 2)[40,41] was conducted. Both MCS provide ~95% average accuracy, which means that the rules created for the calibration spaces allow for predicting the correct concentration with ~95% accuracy.

Fig. 6 illustrates the two MCS [35] with rules extracted from the DT models. In this visualization, rules are represented by rows while columns represent features, and cells refer to rule predicates. These predicates delimit the values of capacitance for *S.aureus* concentrations, while rules are ordered by concentration class and the features are ordered by importance. Figs. 6a and 6b show MCS with five selected frequencies among 19. For *S.aureus* detection in PBS samples in Fig. 6a, 21 Hz is the most important frequency (feature) for biosensing, while 1000 Hz is the most important frequency for *S. aureus* detection in milk samples in Fig. 6b. These features are positioned in the first column of each MCS, with an importance value of 0.33. Furthermore, frequencies are used in the rules which belong to different spectral regions, with the exception of rule r1 for 10^7 CFU/mL (PBS Solution) and for the reference sample (without bacteria) for detection in milk samples. The need to employ different frequency regions supports the usefulness of impedance spectra, as the distinction ability is increased compared to using only electrical responses at given frequencies. The two MCS present the minimum number of rules (i.e. 7, one for each concentration class), thus revealing a strong separability capacity.

4. Conclusions

We reported a selective immunosensor capable of detecting *S. aureus* in buffer solutions and in milk, with a sensitivity that is sufficient for early diagnosis of mastitis in cows. The immunosensor was made with nanostructured films containing a layer of antibodies, which can be produced at low cost. Its usefulness was demonstrated with two principles of detection, viz. electrical and electrochemical impedance spectroscopies, thus indicating that the specific interactions involving antibodies are sufficiently strong to be captured by different methods, including with portable devices. Indeed, with PM-IRRAS we could stablished the molecular-level interactions responsible for the sensing mechanisms. The selectivity of the immunosensor was verified using a series of possible interferents, whose impedance spectra were treated with a multidimensional projection technique. Though distinction of the various samples could be made, there were also changes in the spectra induced by the interferents – probably due to non-specific adsorption. This latter limitation was addressed by employing machine learning to obtain a multidimensional calibration space (MCS) [33] based on decision trees. Using this new construct of analytical chemistry, it was possible to establish rules that provide predictability for employing the immunosensor in detecting *S. aureus* in real samples with intrinsic variability (as in milk). Taken together, the immunosensing and the data processing technologies presented here pave the way for performing on-site early diagnosis of mastitis, in addition to detecting *S. aureus* in food samples.

Declaration of Competing Interest

The authors declare that they have no known competing financial interests or personal relationships that could have appeared to influence the work reported in this paper.

Acknowledgments

This work was supported by CNPq (Grants #103266/2020-8 and #113757/2018-2), São Paulo Research Foundation (FAPESP) (Grants #2018/22214-6 and #2018/18953-8), INEO, SISNANO – MCTI and Agronano Network. The authors also wish to express thanks for the support received from the Qualification Program of the Federal Institute of São Paulo (IFSP), as well as from the Natural Sciences and Engineering Research Council of Canada (NSERC).

Supplementary materials

Supplementary material associated with this article can be found, in the online version, at doi:10.1016/j.snr.2022.100083.

References

[1] H. Jamali, H.W. Barkema, M. Jacques, E.-M. Lavallée-Bourget, F. Malouin, V. Saini, H. Stryhn, S. Dufour, Invited review: Incidence, risk factors, and effects of clinical mastitis recurrence in dairy cows, Journal of Dairy Science 101 (2018) 4729–4746, https://doi.org/10.3168/jds.2017-13730.

[2] J. Côté-Gravel, F. Malouin, Symposium review: Features of Staphylococcus aureus mastitis pathogenesis that guide vaccine development strategies, Journal of Dairy Science 102 (2019) 4727–4740, https://doi.org/10.3168/jds.2018-15272.

[3] Y.S. Mahmmod, I.C. Klaas, S.S. Nielsen, J. Katholm, N. Toft, Effect of presampling procedures on real-time PCR used for diagnosis of intramammary infections with Staphylococcus aureus in dairy cows at routine milk recordings, Journal of Dairy Science 96 (2013) 2226–2233, https://doi.org/10.3168/jds.2012-6059.

[4] R. Riffon, K. Sayasith, H. Khalil, P. Dubreuil, M. Drolet, J. Lagacé, Development of a Rapid and Sensitive Test for Identification of Major Pathogens in Bovine Mastitis by PCR, J Clin Microbiol 39 (2001) 2584–2589, https://doi.org/10.1128/JCM.39.7.2584-2589.2001.

[5] S. Dharmaraj, The Basics: RT-PCR, (n.d.). https://www.thermofisher.com/br/en/home/references/ambion-tech-support/rtpcr-analysis/general-articles/rt-pcr-the-basics.html (accessed July 21, 2021).

[6] R. Rupp, F. Beaudeau, D. Boichard, Relationship between milk somatic-cell counts in the first lactation and clinical mastitis occurrence in the second lactation of French Holstein cows, Preventive Veterinary Medicine 46 (2000) 99–111, https://doi.org/10.1016/S0167-5877(00)00142-2.

[7] R. Antanaitis, V. Juozaitienė, V. Jonike, W. Baumgartner, A. Paulauskas, Milk Lactose as a Biomarker of Subclinical Mastitis in Dairy Cows, Animals 11 (2021) 1736, https://doi.org/10.3390/ani11061736.

[8] N.C. Friggens, M.G.G. Chagunda, M. Bjerring, C. Ridder, S. Hojsgaard, T. Larsen, Estimating Degree of Mastitis from Time-Series Measurements in Milk: A Test of a Model Based on Lactate Dehydrogenase Measurements, Journal of Dairy Science 90 (2007) 5415–5427, https://doi.org/10.3168/jds.2007-0148.

[9] E. Norberg, H. Hogeveen, I.R. Korsgaard, N.C. Friggens, K.H.M.N. Sloth, P. Løvendahl, Electrical Conductivity of Milk: Ability to Predict Mastitis Status, Journal of Dairy Science 87 (2004) 1099–1107, https://doi.org/10.3168/jds.S0022-0302(04)73256-7.

[10] M. Hovinen, H. Simojoki, R. Pösö, J. Suolaniemi, P. Kalmus, L. Suojala, S. Pyörälä, *N* -acetyl -β-D-glucosaminidase activity in cow milk as an indicator of mastitis, Journal of Dairy Research 83 (2016) 219–227, https://doi.org/10.1017/S0022029916000224.

[11] P.R.F. Adkins, J.R. Middleton, Methods for Diagnosing Mastitis, Veterinary Clinics of North America, Food Animal Practice 34 (2018) 479–491, https://doi.org/10.1016/j.cvfa.2018.07.003.

[12] A.C. Soares, J.C. Soares, V.C. Rodrigues, O.N. Oliveira Jr, L.H. Capparelli Mattoso, Controlled molecular architectures in microfluidic immunosensors for detecting Staphylococcus aureus, Analyst 145 (2020) 6014–6023, https://doi.org/10.1039/D0AN00714E.

[13] L.A. Buscaglia, O.N. Oliveira Jr, J.P. Carmo, Roadmap for Electrical Impedance Spectroscopy for Sensing: A Tutorial, IEEE Sensors J (2021), https://doi.org/10.1109/JSEN.2021.3085237, 1–1.

[14] W. Lai, J. Zhuang, D. Tang, Novel Colorimetric Immunoassay for Ultrasensitive Monitoring of Brevetoxin B Based on Enzyme-Controlled Chemical Conversion of Sulfite to Sulfate, J. Agric. Food Chem. 63 (2015) 1982–1989, https://doi.org/10.1021/acs.jafc.5b00425.

[15] Q. Zhou, D. Tang, Recent advances in photoelectrochemical biosensors for analysis of mycotoxins in food, TrAC Trends in Analytical Chemistry 124 (2020), 115814, https://doi.org/10.1016/j.trac.2020.115814.

[16] Y. Lin, Q. Zhou, D. Tang, R. Niessner, H. Yang, D. Knopp, Silver Nanolabels-Assisted Ion-Exchange Reaction with CdTe Quantum Dots Mediated Exciton Trapping for Signal-On Photoelectrochemical Immunoassay of Mycotoxins, Anal. Chem. 88 (2016) 7858–7866, https://doi.org/10.1021/acs.analchem.6b02124.

[17] M. Singh, N. Kaur, E. Comini, The role of self-assembled monolayers in electronic devices, J. Mater. Chem. C. 8 (2020) 3938–3955, https://doi.org/10.1039/D0TC00388C.

[18] Th. Wink, S.J. van Zuilen, A. Bult, W.P. van Bennekom, Self-assembled Monolayers for Biosensors, Analyst 122 (1997) 43R–50R, https://doi.org/10.1039/a606964i.

[19] K. Ariga, Progress in Molecular Nanoarchitectonics and Materials Nanoarchitectonics, Molecules 26 (2021) 1621, https://doi.org/10.3390/molecules26061621.

[20] K. Ariga, E. Ahn, M. Park, B. Kim, Layer-by-Layer Assembly: Recent Progress from Layered Assemblies to Layered Nanoarchitectonics, Chem. Asian J. 14 (2019) 2553–2566, https://doi.org/10.1002/asia.201900627.

[21] J.C. Soares, A.C. Soares, P.A.R. Pereira, V. da C. Rodrigues, F.M. Shimizu, M. E. Melendez, C. Scapulatempo Neto, A.L. Carvalho, F.L. Leite, S.A.S. Machado, O. N. Oliveira Jr, Adsorption according to the Langmuir–Freundlich model is the detection mechanism of the antigen p53 for early diagnosis of cancer, Physical Chemistry Chemical Physics 18 (2016) 8412–8418, https://doi.org/10.1039/C5CP07121F.

[22] O.N. Oliveira Jr, R.M. Iost, J.R. Siqueira, F.N. Crespilho, L. Caseli, Nanomaterials for Diagnosis: Challenges and Applications in Smart Devices Based on Molecular Recognition, ACS Appl. Mater. Interfaces. 6 (2014) 14745–14766, https://doi.org/10.1021/am5015056.

[23] Y. Lin, Q. Zhou, D. Tang, R. Niessner, D. Knopp, Signal-On Photoelectrochemical Immunoassay for Aflatoxin B $_1$ Based on Enzymatic Product-Etching MnO $_2$ Nanosheets for Dissociation of Carbon Dots, Anal. Chem. 89 (2017) 5637–5645, https://doi.org/10.1021/acs.analchem.7b00942.

[24] N. Arroyo-Currás, K. Scida, K.L. Ploense, T.E. Kippin, K.W. Plaxco, High Surface Area Electrodes Generated via Electrochemical Roughening Improve the Signaling of Electrochemical Aptamer-Based Biosensors, Anal. Chem. 89 (2017) 12185–12191, https://doi.org/10.1021/acs.analchem.7b02830.

[25] S.Y. Kim, J.-C. Lee, G. Seo, J.H. Woo, M. Lee, J. Nam, J.Y. Sim, H.-R. Kim, E. C. Park, S. Park, Computational Method-Based Optimization of Carbon Nanotube Thin-Film Immunosensor for Rapid Detection of SARS-CoV-2 Virus, Small Science (2021), 2100111, https://doi.org/10.1002/smsc.202100111.

[26] K. Ariga, M. Nishikawa, T. Mori, J. Takeya, L.K. Shrestha, J.P. Hill, Self-assembly as a key player for materials nanoarchitectonics, Science and Technology of Advanced Materials 20 (2019) 51–95, https://doi.org/10.1080/14686996.2018.1553108.

[27] K. Ariga, E. Ahn, M. Park, B. Kim, Layer-by-Layer Assembly: Recent Progress from Layered Assemblies to Layered Nanoarchitectonics, Chem. Asian J. 14 (2019) 2553–2566, https://doi.org/10.1002/asia.201900627.

[28] J. Xiong, Z. Zheng, X. Qin, M. Li, H. Li, X. Wang, The thermal and mechanical properties of a polyurethane/multi-walled carbon nanotube composite, Carbon 44 (2006) 2701–2707, https://doi.org/10.1016/j.carbon.2006.04.005.

[29] A.C. Soares, J.C. Soares, F.M. Shimizu, M.E. Melendez, A.L. Carvalho, O.N. Oliveira Jr, Controlled Film Architectures to Detect a Biomarker for Pancreatic Cancer Using Impedance Spectroscopy, ACS Applied Materials & Interfaces 7 (2015) 25930–25937, https://doi.org/10.1021/acsami.5b08666.

[30] A.C. Soares, Filmes nanoestruturados aplicados em biossensores para detecção precoce de câncer de pâncreas, Universidade de São Paulo, 2017.

[31] J.C. Soares, F.M. Shimizu, A.C. Soares, L. Caseli, J. Ferreira, O.N. Oliveira Jr, Supramolecular Control in Nanostructured Film Architectures for Detecting Breast Cancer, ACS Applied Materials & Interfaces 7 (2015) 11833–11841, https://doi.org/10.1021/acsami.5b03761.

[32] R. Minghim, F.V. Paulovich, A. de Andrade Lopes, Content-based text mapping using multi-dimensional projections for exploration of document collections, in: R. F. Erbacher, J.C. Roberts, M.T. Gröhn, K. Börner (Eds.), San Jose, CA, 2006: p. 60600S. https://doi.org/10.1117/12.650880.

[33] M. Popolin-Neto, A.C. Soares, O.N. Oliveira Jr, F.V. Paulovich, Machine Learning Used to Create a Multidimensional Calibration Space for Sensing and Biosensing Data, BCSJ 94 (2021) 1553–1562, https://doi.org/10.1246/bcsj.20200359.

[34] R. Salman, V. Kecman, Regression as classification, in: 2012 Proceedings of IEEE Southeastcon, IEEE, Orlando, FL, USA, 2012, pp. 1–6, https://doi.org/10.1109/SECon.2012.6196887.

[35] M. Popolin-Neto, F.V. Paulovich, Explainable Matrix - Visualization for Global and Local Interpretability of Random Forest Classification Ensembles, IEEE Trans. Visual. Comput. Graphics. 27 (2021) 1427–1437, https://doi.org/10.1109/TVCG.2020.3030354.

[36] L. Breiman, Classification and regression trees, 1. CRC Press repr, Chapman & Hall/CRC, Boca Raton, Fla, 1998.

[37] P.-N. Tan, M. Steinbach, V. Kumar, Introduction to data mining, 1st ed, Pearson Addison Wesley, Boston, 2006.

[38] G. James, D. Witten, T. Hastie, R. Tibshirani, An Introduction to Statistical Learning, Springer New York, New York, NY, 2013. https://doi.org/10.1007/978-1-4614-7138-7.

[39] C.S. Mellish, in: Proceedings of the Fourteenth International Joint Conference on Artificial Intelligence, Morgan Kaufmann, San Mateo, Calif, 1995.

[40] S. Varma, R. Simon, Bias in error estimation when using cross-validation for model selection, BMC Bioinformatics 7 (2006) 91, https://doi.org/10.1186/1471-2105-7-91.

[41] I. Tsamardinos, A. Rakhshani, V. Lagani, Performance-Estimation Properties of Cross-Validation-Based Protocols with Simultaneous Hyper-Parameter Optimization, in: A. Likas, K. Blekas, D. Kalles (Eds.), Artificial Intelligence: Methods and Applications, Springer International Publishing, Cham, 2014, pp. 1–14, https://doi.org/10.1007/978-3-319-07064-3_1.

[42] N.B. Colthup, L.H. Daly, S.E. Wiberley, Introduction to infrared and Raman spectroscopy, 3rd ed, Academic Press, Boston, 1990.

[43] A. Więckowski, C. Korzeniewski, B. Braunschweig (Eds.), Vibrational spectroscopy at electrified interfaces, Wiley, Hoboken, New Jersey, 2013.

[44] S. Johler, R. Stephan, D. Althaus, M. Ehling-Schulz, T. Grunert, High-resolution subtyping of Staphylococcus aureus strains by means of Fourier-transform infrared spectroscopy, Systematic and Applied Microbiology 39 (2016) 189–194, https://doi.org/10.1016/j.syapm.2016.03.003.

[45] T. Grunert, M. Wenning, M.S. Barbagelata, M. Fricker, D.O. Sordelli, F.R. Buzzola, M. Ehling-Schulz, Rapid and Reliable Identification of Staphylococcus aureus Capsular Serotypes by Means of Artificial Neural Network-Assisted Fourier Transform Infrared Spectroscopy, Journal of Clinical Microbiology 51 (2013) 2261–2266, https://doi.org/10.1128/JCM.00581-13.

[46] S. Karimi, J. Feizy, F. Mehrjo, M. Farrokhnia, Detection and quantification of food colorant adulteration in saffron sample using chemometric analysis of FT-IR spectra, RSC Adv 6 (2016) 23085–23093, https://doi.org/10.1039/C5RA25983E.

[47] U. Böcker, S.G. Wubshet, D. Lindberg, N.K. Afseth, Fourier-transform infrared spectroscopy for characterization of protein chain reductions in enzymatic reactions, Analyst 142 (2017) 2812–2818, https://doi.org/10.1039/C7AN00488E.

[48] V. Erukhimovitch, V. Pavlov, M. Talyshinsky, Y. Souprun, M. Huleihel, FTIR microscopy as a method for identification of bacterial and fungal infections, Journal of Pharmaceutical and Biomedical Analysis 37 (2005) 1105–1108, https://doi.org/10.1016/j.jpba.2004.08.010.

[49] N. Nicolaou, Y. Xu, R. Goodacre, Fourier transform infrared spectroscopy and multivariate analysis for the detection and quantification of different milk species, Journal of Dairy Science 93 (2010) 5651–5660, https://doi.org/10.3168/jds.2010-3619.

[50] S.C. Das, S. Guin, A.K. Ghosh, J. Metra, D. Kumar, K. Mitra, S.K. Das, Evaluation of total bacterial count (TBC) and somatic cell count (SCC) for detection of latent and sub-clinical mastitis in cow and buffalo, The Indian Journal of Animal Sciences 78 (2008) 827–829.

[51] V.C Rodrigues, C.H Comin, J.C Soares, A.C Soares, M.E Melendez, J.H.T. G Fregnani, A.L Carvalho, L.F. Costa, O.N Oliveira Jr, Analysis of Scanning Electron Microscopy Images To Investigate Adsorption Processes Responsible for Detection

of Cancer Biomarkers, ACS Appl. Mater. Interfaces 9 (7) (2017) 5885–5890, https://doi.org/10.1021/acsami.6b16105.